Mercury's rotational parameters from MESSENGER image and laser altimeter data: A feasibility study

Alexander Stark [a,b], Jürgen Oberst [a,c], Frank Preusker [a], Klaus Gwinner [a], Stanton J. Peale [d], Jean-Luc Margot [e,f], Roger J. Phillips [g], Maria T. Zuber [h], Sean C. Solomon [i,j]

[a] German Aerospace Center, Institute of Planetary Research, D-12489 Berlin, Germany, [b] Technische Universität Berlin, Institute of Geodesy and Geoinformation Science, D-10623 Berlin, Germany, [c] Moscow State University for Geodesy and Cartography, RU-105064 Moscow, Russia, [d] Department of Physics, University of California, Santa Barbara, CA 93106, USA, [e] Department of Earth, Planetary, and Space Sciences, University of California, Los Angeles, CA 90095, USA, [f] Department of Physics and Astronomy, University of California, Los Angeles, CA 90095, USA, [g] Southwest Research Institute, Boulder, CO 80302, USA, [h] Department of Earth, Atmospheric and Planetary Sciences, Massachusetts Institute of Technology, Cambridge, MA 02139, USA, [i] Lamont-Doherty Earth Observatory, Columbia University, Palisades, NY 10964, USA, [j] Department of Terrestrial Magnetism, Carnegie Institution of Washington, Washington, DC 20015, USA

The final publication is available at Elsevier via http://dx.doi.org/10.1016/j.pss.2015.05.006.

Abstract

A novel method has been developed to determine the rotational parameters of Mercury from data acquired by the MESSENGER spacecraft. We exploit the complementarity of laser altimeter tracks taken at different rotational phases and rigid stereo terrain models to determine a Mercury rotational model. In particular, we solve for the orientation of the spin axis, the rotation rate, and the amplitude of the forced libration. In this paper, we verify the proposed method and carry out an extensive simulation of MESSENGER data acquisition with assumed rotational parameters. To assess the uncertainty in the rotational parameters we use mission-typical assumptions for spacecraft attitude and position knowledge as well as for small-scale terrain morphology. We find that the orientation of the spin axis and the libration amplitude can be recovered with an accuracy of a few arc seconds from three years of MESSENGER orbital observations. The rotation rate can be determined to within 5 arc seconds per year. The method developed here serves as a framework for the ongoing analysis of data from the MESSENGER spacecraft. The rotational parameters of Mercury hold important constraints on the internal structure and evolution of the planet.

1 Introduction

Mercury, located deep in the gravity well of the Sun, displays distinctive dynamics. The rotation and orbital motion of the planet are tidally coupled, and Mercury rotates precisely three times for every two revolutions about the Sun. In addition to its mean rotation, the planet displays small forced librations in longitude, i.e., oscillations about the average rotation rate. Measurements of rotational parameters are of considerable interest, as the amplitude of the forced libration and the planet's obliquity provide (when combined with gravity field parameters) important constraints on the planet's interior structure (*Peale*, 1976, 1988; *Margot et al.*, 2012; *Smith et al.*, 2012; *Hauck et al.*, 2013). This situation thus offers an opportunity to derive information about a planet's interior, particularly the size and state of the planetary core, not easily accessible for other planets of the Solar System family.

Measurements of Mercury's librations and obliquity with Earth-based radar revealed a large libration amplitude (approximately 450 m at the equator), suggesting that Mercury's core is at least partially molten (*Margot et al.*, 2007, 2012). With this method, instantaneous spin rate values are obtained from radar time-lag measurements, which have provided the most accurate measurements of the spin rate variations to date. However, the precision remains somewhat limited and prevents the detection of small variations, such as those expected from long-period librations (*Peale et al.*, 2007; *Yseboodt et al.*, 2010).

Several other techniques have been proposed to measure the rotational parameters of Mercury. An obvious approach is to use images from different rotation phases and apply image correlation techniques to constrain the unknown rotation parameters (*Wu et al.*, 1997; *Jehn et al.*, 2004; *Pfyffer et al.*, 2011). However, precise camera attitude and spacecraft position information must be available for this approach to be feasible. Alternative methods make use of laser altimetric cross-over points (*Rosat et al.*, 2008) or employ a separation of the dynamic and static topography by spherical harmonic expansion of the latter (*Koch et al.*, 2008, 2010). Observations of Mercury's gravitational field can also be used to determine the rotational parameters (*Cicalò and Milani*, 2012; *Mazarico et al.*, 2014). This technique requires precise radio tracking and modeling of non-conservative forces acting on the spacecraft. However, as the dynamics of the gravity field can be influenced by differential rotation of the core, the combination of shape and core rotation could provide more information about the interior structure than either quantity alone.

Here we investigate the quality of measurements obtained by the MErcury Surface, Space ENvironment, GEochemistry, and Ranging (MESSENGER) spacecraft. Precise measurements of a planet's rotation rate from an orbiting platform

are far from straightforward, as, for example, a fixed reference against which the rotation can be observed is not readily available. Knowledge of a spacecraft's orbit and instrument pointing data suffer from errors that make the accurate measurement of small libration effects challenging. The application of these methods to MESSENGER data is complicated by the spacecraft's highly eccentric orbit and observational constraints for the instruments set by that orbit as well as by limitations on spacecraft attitude relative to the planet-Sun line. Our new approach combines the benefits of both laser altimetry and stereo imaging to overcome their individual drawbacks. In particular, we discuss the combination of time-dependent, high-accuracy range measurements by the laser altimeter with the static terrain data obtained from stereo images.

In order to assess the potential as well as the limitations of our approach we carry out an extensive simulation of MESSENGER data. We adopt a given topographic model, derived from MESSENGER stereo images, and we perform a simulation of laser altimeter observations given an assumed rotational model for Mercury (see Fig. 1). Then, an attempt is made to recover the rotational parameters by analysis of the simulated data. This simulation serves as a basis for future analysis of actual data acquired by MESSENGER's instruments and the estimation of the rotational parameters of Mercury from those data.

The paper is structured as follows. First we describe the available data from MESSENGER, concentrating specifically on laser altimeter profiles and topographic models generated from stereo images. In the subsequent section we report on forward modeling to generate synthetic laser altimeter profiles. Finally, we describe our method for the measurement of rotational parameters and the results obtained with the simulation.

2 MESSENGER data

MESSENGER was inserted into orbit about Mercury in March 2011. Its initial orbit was highly eccentric and near-polar, with a 12 h period. In April 2012, the orbit period was shortened in two propulsive maneuvers to 8 h. For our study, we use data from the Mercury Laser Altimeter (MLA) (*Cavanaugh et al.*, 2007) and the Mercury Dual Imaging System (MDIS) (*Hawkins et al.*, 2007). We next describe the data obtained by these instruments.

2.1 Laser altimeter

MLA carries out its measurements along approximately great-circle profiles, as the spacecraft moves along its orbit track. With a pulse energy of 20 mJ, the instrument can range from altitudes as great as 1500 km in the nadir orientation

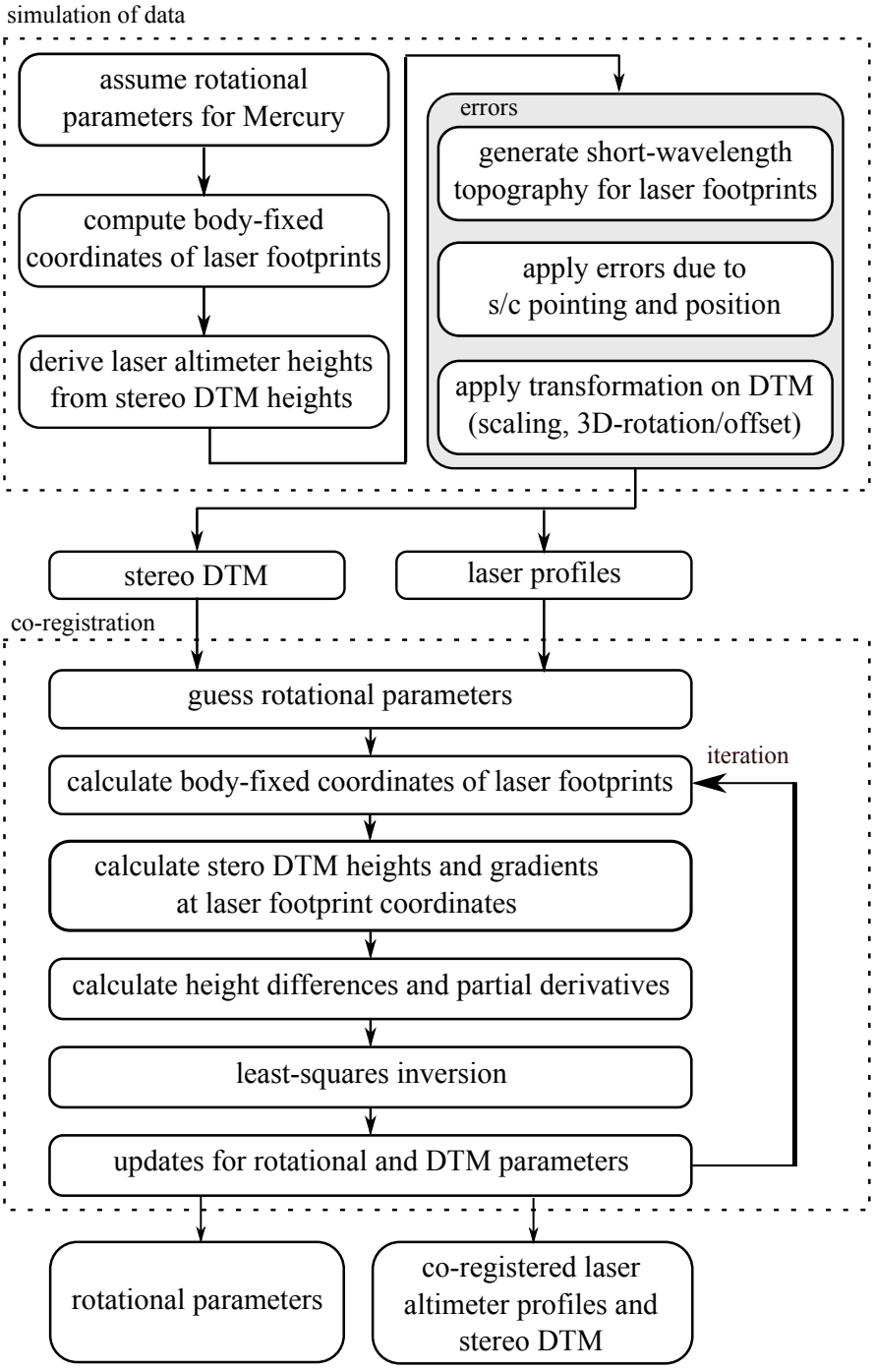

Figure 1: Scheme of the simulation of observational data and determination of rotational parameters (s/c denotes spacecraft, and 3D denotes three-dimensional).

and to distances as great as 1000 km at an off-nadir angle of 40° (*Zuber et al.*, 2008, 2012). The along-track resolution of the measurements is determined by the size and spacing of the laser footprints on the surface. The distance between footprints at the 8 Hz pulse repetition rate varies with the velocity of the spacecraft between 170 m and 440 m. Depending on the ranging distance, the laser footprint diameters vary from 16 m to 134 m. As of August 2013, after an observation time of 850 days, MLA had acquired 1768 laser profiles that span the latitude range from 90° N to 20° S.

In our simulation, we used laser profiles over a small area of Mercury's surface, for which a digital terrain model (DTM) derived from stereo images is available. The area extends in latitude from 25 to 65° N and in longitude from 190 to 270° E. Clearly, the final accuracy of the rotational parameters will depend on the size of the DTM area considered and the number of laser altimeter observations within that area.

2.2 Stereo photogrammetry

We define the topography represented by the stereo DTM as the length of the local planetary radius from the center of mass of Mercury to the surface, relative to the radius of a reference sphere, here taken as 2440 km.

The production of a DTM from stereo images follows established procedures (*Gwinner et al.*, 2010; *Preusker et al.*, 2011). With the benefit of image correlation and least-squares block adjustment techniques, we concatenated large numbers of images, and we obtained a terrain model with high internal geometric accuracy and rigidity. On the other hand, the absolute position of a local DTM with respect to Mercury's center of mass is uncertain, and the DTM may show small lateral and vertical offsets as well as tilts with respect to the Mercury-fixed reference frame.

For our study we used a DTM reconstructed from more than 2500 individual MDIS images. Fig. 2 shows a part of the DTM along with the coverage of the same area by MLA. To minimize distortion by the map projection, in our calculations we used a Lambert conic conformal projection with two standard parallels. The DTM is available as a structured map grid with a lateral resolution of 222 m. Although the size of an individual grid element is typically determined by the resolution of the images that were used to generate the terrain model, the effective resolution (i.e., the size of the smallest topographic feature resolved by the DTM) may be larger (see 4.2 below). The vertical resolution of the DTM is about 60 m.

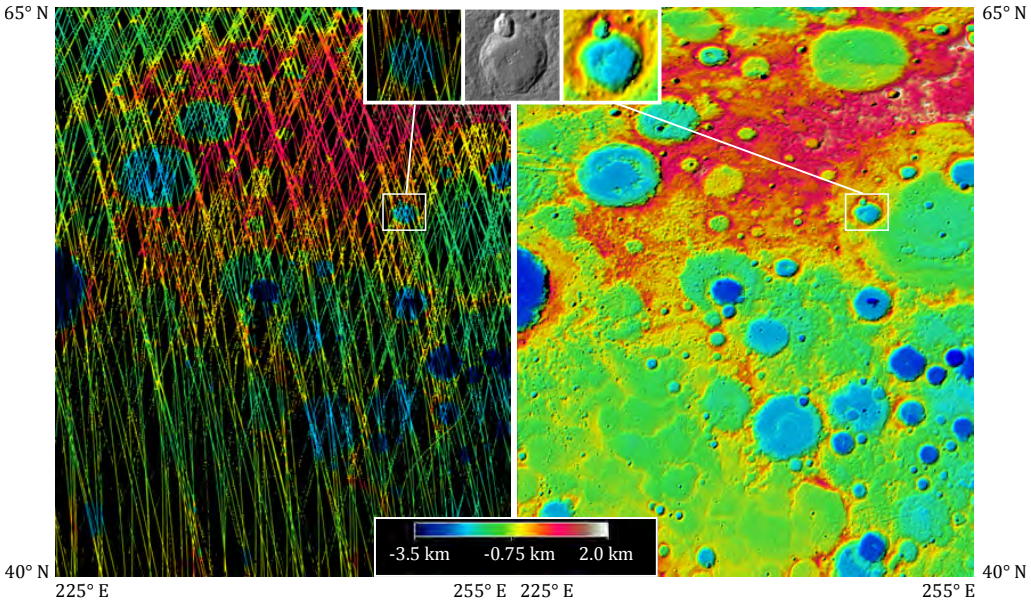

Figure 2: (Left) MLA coverage as of August 2013 of a part (20%) of the area considered in this study. (Right) The same area reconstructed in a stereo DTM. Both maps share the same color bar. The inset shows detailed views of an unnamed crater (centered at 56.6° N, 24° E and enclosed in a white box on both panels) along with an MDIS image (EW0226964842G).

3 Rotational model of Mercury

The rotational parameters consist of a set of values defining the orientation of Mercury with respect to a given reference frame at a given epoch. In this study we determined the rotational elements at J2000.0 with respect to the International Celestial Reference Frame (ICRF). The ICRF is approximately (within 0.1 arc sec) the reference frame of the mean Earth equator and equinox of the J2000 epoch (*Archinal et al.*, 2011). The orientation of Mercury's spin axis is described by the right ascension α_0 and declination δ_0 of the intercept of the rotational axis vector with the celestial sphere. The precession of the spin axis is predicted to have a period of around 300,000 years (*Yseboodt and Margot*, 2006; *Stark et al.*, 2015) and is described by α_1 and δ_1 (expressed in degrees per unit time). The coordinates of Mercury's north pole with respect to the ICRF at a given time t are given by the angles

$$\alpha(t) = \alpha_0 + \alpha_1 t \qquad \text{and} \qquad \delta(t) = \delta_0 + \delta_1 t\,, \tag{1}$$

where the time is measured with respect to the J2000.0 epoch. The rotation of the planet around its spin axis is described by

$$\omega(t) = \omega_0 + \omega_1 t + \sum_k g_{(88/k)} \sin(k n_0 (t + t_0))\,, \tag{2}$$

where ω_0 is the prime meridian constant, ω_1 is the rotation rate, and the last term is the physical libration in longitude (*Margot*, 2009; *Yseboodt et al.*, 2010). The latter is composed from the superposition of k harmonics of the orbital frequency. The libration is parameterized by the amplitude of the kth harmonic $g_{(88/k)}$, the mean motion $n_0 = 4.09233445^\circ/\text{day}$, and the time offset that ties the libration phase to the J2000.0 epoch, $t_0 = 42.71182$ days. The amplitudes of the harmonics are related by

$$g_{(88/(k+1))} = g_{(88/k)} \frac{G_{(201)}(k+1,e)}{G_{(201)}(k,e)}, \tag{3}$$

where $G_{(201)}(k,e) = (G_{(201-k)}(e) - G_{(201+k)}(e))/k^2$ is the difference between two Kaula eccentricity functions (*Kaula*, 2000) and $e = 0.2056317$ is Mercury's orbital eccentricity (*Stark et al.*, 2015). Given the amplitude of the fundamental frequency g_{88}, the amplitudes of the higher harmonics can be derived with Eq. 3. The sum in Eq. 2 is truncated at $k = 5$, neglecting libration terms with amplitudes below 10^{-3} arc sec.

In our treatment of the rotation of the planet we neglected any long-term (more than 88 days) longitudinal librations. It is expected that because of a resonance effect the perturbation of Mercury's orbit by Jupiter can lead to an 11.86-yr libration with an amplitude comparable to that of the annual libration (*Peale et al.*, 2007; *Yseboodt et al.*, 2010). However, during the observation time considered in this work any long-term libration will appear only as an increase or decrease of the mean spin rate ω_1, which is already a parameter of the model. The same holds for the precession rates, which we do not attempt to determine but assume to be fixed at $\alpha_1 = -0.032808^\circ$ per century and $\delta_1 = -0.0048464^\circ$ per century (*Stark et al.*, 2015). Any changes in the value of the prime meridian constant ω_0 are equivalent to a rotation around the polar axis. This rotation will be treated elsewhere, and the prime meridian constant is fixed at $\omega_0 = 329.5469^\circ$.

4 Simulation of topographic observations

The simulation, outlined in Fig. 1, was conducted as follows. First, from a user-defined rotation model (Table 1), body-fixed coordinates of the MLA footprints were obtained. At these positions we determined the corresponding heights from the stereo DTM derived from MDIS images. We then performed a simulation of MLA measurements across this DTM. To obtain a realistic simulation, we started with the known spacecraft position and attitude and applied typical errors to both quantities (see Section 4.1). To account for the higher spatial resolution of the MLA measurements, we simulated short-wavelength topography by signal synthesis from a random but appropriately distributed power spectrum for topography (see Section 4.2). Finally, as the DTM is also part of the simulation,

we applied a similarity transformation to the DTM, leading to different reference systems for the laser footprints and the DTM. From the simulation we obtained a set of simulated laser profiles and a stereo DTM, which were used for the co-registration and the recovery of rotational parameters (see Section 5).

4.1 Errors in spacecraft position and attitude

The conditions on spacecraft navigation and instrument operation in orbit about Mercury are challenging. The spacecraft is affected by strong and variable solar radiation and planetary thermal flux. The spacecraft must keep its sunshade pointed toward the Sun to within a tolerance of $\pm 10^\circ$ in pitch and yaw, and a series of attitude changes, many of which result in off-nadir pointing for the MLA, must be performed on every orbit. These off-nadir observations have greater uncertainties in the laser footprint positions. Further, precise orbit information is mandatory to transform laser range measurements to heights on the planet. The reconstruction of MESSENGER's orbit position is complicated by the spacecraft's eccentric orbit and limitations to radio-tracking observations arising from proximity to the Sun. All of these systematic errors can influence the estimation of the rotational parameters.

Typically, cross- and along-track orbit errors are higher than the radial errors. We conservatively assume that radial errors are smaller than 10 m and lateral position errors are smaller than 250 m (*Srinivasan et al.*, 2007). The uncertainty in the spacecraft attitude over an observation time of 0.1 s (pointing jitter) is assumed to be smaller than 15 μrad, and the attitude knowledge error is assumed to be smaller than 250 μrad (*Santo et al.*, 2001). The post-launch alignment of MLA with respect to a spacecraft-fixed coordinate system was determined with passive scans during MESSENGER's Earth flyby in 2005 (*Smith et al.*, 2006). We assume that the remaining alignment error is approximately 500 μrad. Because attitude knowledge and alignment error can compensate each other, a conservative estimate of the total MLA boresight error is given by $\sqrt{(250\,\mu\text{rad})^2 + (500\,\mu\text{rad})^2} = 560\,\mu\text{rad}$. All errors are given by one standard deviation (1σ), i.e., a 68% confidence level, and are assumed to follow a Gaussian distribution.

The spacecraft position and attitude errors are presumed to remain fixed within the short (< 11 min) acquisition time of an individual laser altimeter profile over the stereo DTM. The consideration of measurement conditions allows us to simulate possible correlations between the observational uncertainties and the rotational parameters.

4.2 High-resolution topography

Because MLA measurements typically are superior in height resolution to the stereo-derived DTM, we generated artificial high-resolution topography (on the scale of the laser footprint) beyond the resolution of the DTM. Following methods described by *Preusker et al.* (2011), we first derived the "effective resolution" of the stereo DTM by comparing it with the laser profiles. For the DTM under study with its grid size of 222 m we obtained an effective horizontal resolution of 3.8 km. For further insight, we co-registered actual MLA profiles and the stereo DTM (see Section 5) and performed a Fourier analysis of the residuals. In the frequency spectrum we can observe two regimes (Fig. 3, top) that are separated by the effective DTM resolution. Short-wavelength topography, not realized in the DTM, follows a power-law relation between wavelength and amplitude, whereas residuals at longer wavelengths produce approximately white noise in the spectrum.

We generated synthetic laser altimeter measurements for each MLA profile from randomly generated power spectra having variances that obey the power-wavelength relationship we found from actual data (see Fig. 3, top). After signal synthesis from the spectrum, we obtained simulated height residuals for each MLA "measurement". By adding these residuals to the DTM heights, we produced a laser profile that follows the DTM heights but has an additional synthetic topography with a much finer artificial resolution than the effective resolution of the DTM (Fig. 3, bottom).

4.3 Stereo model

We applied offsets to the stereo DTM, as they are typically observed in stereo image processing. In particular, we carried out a seven-parameter similarity transformation, and we shifted the DTM by a three-dimensional offset vector and applied a rotation and scaling (see Section 5). The offset vector is $(t_x, t_y, t_z) = (400\,\mathrm{m}, 200\,\mathrm{m}, -700\,\mathrm{m})$. The quaternion forming the similarity transformation is $(q_0, q_1, q_2, q_3) = (1.0002, 0.00004, 0.00005, 0.0006)$. This quaternion corresponds to a scaling factor of 1.0004 and a sequential rotation of about 16.5 arc sec, 20.6 arc sec, and 24.7 arc sec around the x-, y-, and z-axes of the body-fixed Mercury frame, respectively, where the x-, y-, and z-axes are in the direction 0°N, 0°E; 0°N, 90°E; and 90°N from the planet center, respectively. This transformation accounts for the different observational and instrumental errors of the MDIS and MLA instruments. The effect of this assumed deformation on height residuals is visualized in Fig. 4 (left panels).

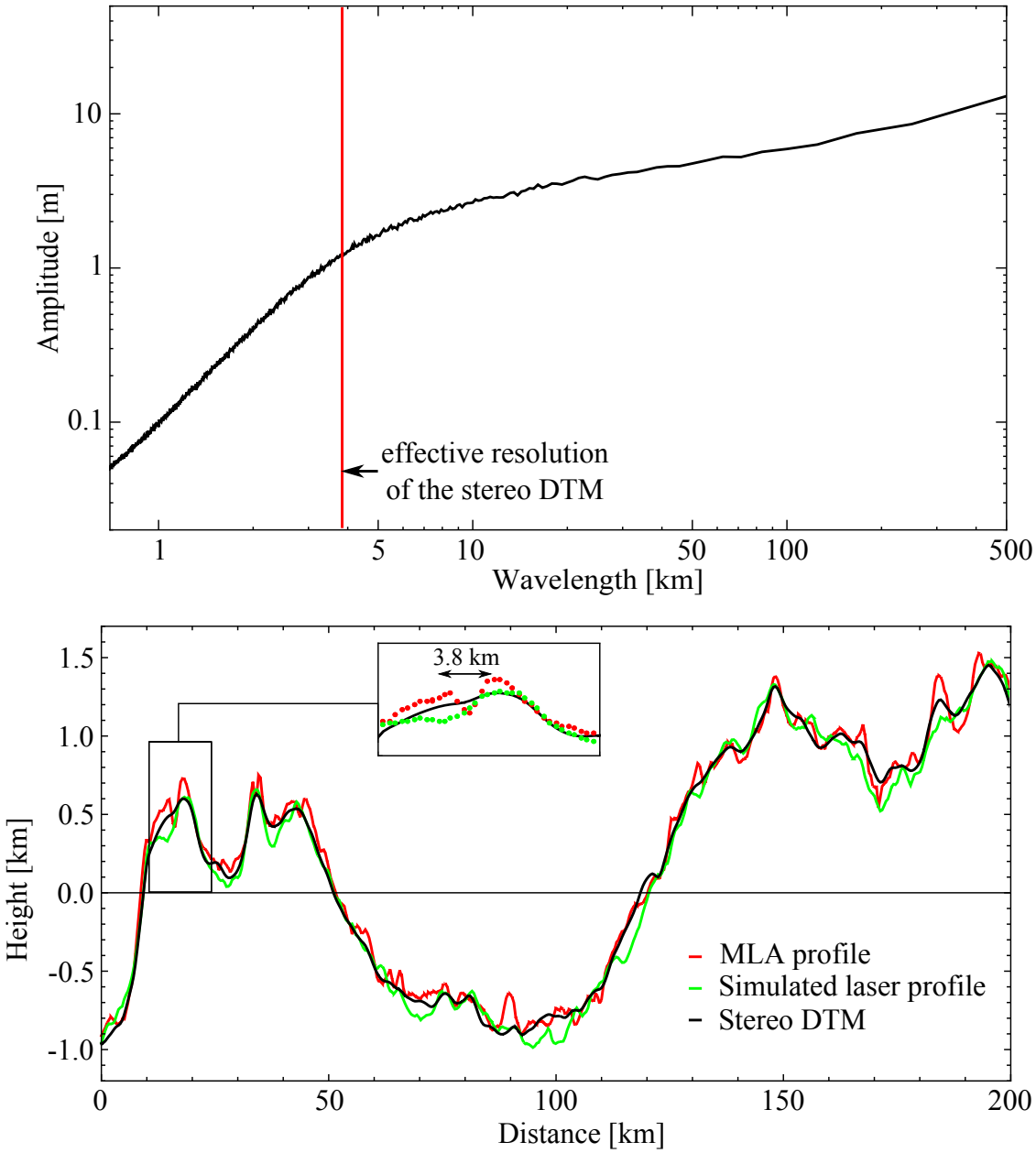

Figure 3: (Top) Averaged power spectrum of the height residuals of MLA profiles along the stereo DTM obtained by a discrete Fourier transform. The red line marks the position of the "effective resolution" of the DTM at 3.8 km. (Bottom) Simulated laser altimeter profile (green) along with actual MLA measurements (red) and stereo DTM heights (black). The inset shows a zoomed view of a portion of the profile; the arrow indicates the "effective resolution" of the DTM.

5 Determination of rotational parameters

In the next step, we used the generated synthetic data and attempted to recover the rotational parameters. The key to this step is the co-registration of laser altimeter tracks to the stereo DTM. Thereby we relate a time-dependent, spatially distributed set of laser altimeter footprints to a static and rigid stereo DTM.

Several techniques for co-registration or comparison of laser altimetry and photogrammetrically derived topography have been proposed (e.g., *Habib and Schenk* (1999); *Baltsavias* (1999); *Postolov et al.* (1999)). Such techniques have been successfully applied to laser altimeter data and stereo topographic models for Mars and the Moon (*Lin et al.*, 2010; *Wu et al.*, 2013; *Gläser et al.*, 2013). In this work we generalized and extended the method developed by *Gläser et al.* (2013) to the determination of dynamical parameters of a rotating body.

The goal of the co-registration is to find a transformation that relates the reference system of the laser altimeter tracks to the reference system of the stereo DTM. Our approach is to co-register points in three dimensions to a quasi-continuous representation of the surface. For this reason we prefer to solve for the transformation from the laser altimeter points, $\mathbf{r}_{\mathrm{LA}}$, to the stereo DTM points, $\mathbf{r}_{\mathrm{DTM}}$, although it is the laser altimetry that provides a reliable absolute reference. After the co-registration is performed, it is straightforward to transform the stereo DTM points to the reference frame of the laser altimeter points.

In order to perform the co-registration we assume that the data sets are related by a three-dimensional similarity transformation with seven parameters: a scaling factor, three rotations, and a translation vector $\mathbf{t} = (t_x, t_y, t_z)$. The scaling and the rotations are performed by the matrix $\mathbf{R}_q$, which is parameterized by a quaternion $\mathbf{q} = (q_0, q_1, q_2, q_3)$. The seven parameters of the transformation are $\mathbf{p}^{\mathrm{DTM}} = (q_0, q_1, q_2, q_3, t_x, t_y, t_z)$. The transformed laser altimeter points $\mathbf{r}^i_{\mathrm{tLA}}$ are given by

$$\mathbf{r}^i_{\mathrm{tLA}} = \mathbf{R}_{\mathrm{q}} \left(\mathbf{r}^i_{\mathrm{LA}} + \mathbf{t} \right) , \tag{4}$$

where i is the index for each of the n laser altimeter points used in the co-registration. The body-fixed coordinates of the laser altimeter points $\mathbf{r}^i_{\mathrm{LA}}$ are calculated via a rotation matrix $\mathbf{R}$ from the inertial points $\mathbf{r}^i_{\mathrm{iLA}}$ by $\mathbf{r}^i_{\mathrm{LA}} = \mathbf{R}\, \mathbf{r}^i_{\mathrm{iLA}}$. The rotation matrix $\mathbf{R}$, i.e., a unitary transformation from inertial to body-fixed coordinates, is a composite of three rotations

$$\mathbf{R} = \mathbf{R_z}(\omega(t^i))\, \mathbf{R_x}(\delta(t^i))\, \mathbf{R_z}(\alpha(t^i)) , \tag{5}$$

where $\mathbf{R_x}$ and $\mathbf{R_z}$ are rotations around the X- and Z-axes of the ICRF inertial frame, respectively. The time-dependent angles α, δ, and ω define a rotation model (Eqs. 1 and 2) and are evaluated at the time t^i when the laser pulse

hits the surface. The rotation parameters are $\mathbf{p}^{\text{rot}} = (\alpha_0, \delta_0, \omega_1, g_{88})$. Consequently, the transformed points are related to the inertial laser altimeter points by $\mathbf{r}^i_{\text{tLA}} = \mathbf{R}_\mathbf{q}(\mathbf{R}\,\mathbf{r}^i_{\text{iLA}} + \mathbf{t})$.

When an optimal set of parameters is found, the radial component of the transformed points $\left|\mathbf{r}^i_{\text{tLA}}\right|$ should be identical to the DTM heights, $r^i_{\text{DTM}} = \left|\mathbf{r}^i_{\text{DTM}}\right|$. We use radial differences as residuals to be minimized. Hence, the functional model $g(\mathbf{p})$ for the co-registration is given by

$$\mathbf{g}^i(\mathbf{p}) = r^i_{\text{DTM}}(\lambda^i(\mathbf{p}), \phi^i(\mathbf{p})) - \left|\mathbf{r}^i_{\text{tLA}}(\mathbf{p})\right| , \tag{6}$$

where $\mathbf{p} = (\mathbf{p}^{\text{rot}}, \mathbf{p}^{\text{DTM}})$ is the parameter vector containing the transformation $\mathbf{p}^{\text{DTM}}$ and the rotation parameters $\mathbf{p}^{\text{rot}}$. The DTM heights r^i_{DTM} are obtained at the coordinates of the transformed points, $\mathbf{r}^i_{\text{tLA}}$, i.e., the latitude λ^i and longitude ϕ^i. These coordinates are obtained from the inertial coordinates $\mathbf{r}^i_{\text{iLA}}$ and the rotation parameters $\mathbf{p}^{\text{rot}}$.

The optimal parameters of this heavily overdetermined problem are obtained iteratively from (*Tarantola and Valette*, 1982)

$$\mathbf{p}_{k+1} = \mathbf{p}_k - \left(\mathbf{G}_k \mathbf{C}_g^{-1} \mathbf{G}_k^{\text{T}}\right)^{-1} \mathbf{G}_k^{\text{T}} \mathbf{C}_g^{-1} \mathbf{g}(\mathbf{p}_k) , \tag{7}$$

where $\mathbf{C}_g$ is the weighting matrix of the observations (see Section 6), and T denotes transpose. The matrix of partial derivatives $\mathbf{G}$ is built from the gradients of the stereo DTM heights

$$G_{ij} = \frac{\partial g^i(\mathbf{p})}{\partial p_j} = \left(\frac{\partial r^i_{\text{DTM}}}{\partial \lambda}\right) \frac{\partial \lambda}{\partial p_j} + \left(\frac{\partial r^i_{\text{DTM}}}{\partial \phi}\right) \frac{\partial \phi}{\partial p_j} - \frac{\partial \left|\mathbf{r}^i_{\text{tLA}}\right|}{\partial p_j} \tag{8}$$

and is recalculated every iteration. By using $\mathbf{r}^i_{\text{tLA}} = (x, y, z)$, $r = \left|\mathbf{r}^i_{\text{tLA}}\right|$, $\rho = \sqrt{x^2 + y^2}$, $\lambda = \arcsin(z/r)$, and, $\phi = \arctan(y, x)$ we obtain

$$G_{ij} = \left[\left(\frac{\partial r^i_{\text{DTM}}}{\partial \lambda}\right) \frac{1}{r^2 \rho} \begin{pmatrix} -zx \\ -zy \\ \rho^2 \end{pmatrix} + \left(\frac{\partial r^i_{\text{DTM}}}{\partial \phi}\right) \frac{1}{\rho^2} \begin{pmatrix} -y \\ x \\ 0 \end{pmatrix} - \frac{1}{r} \begin{pmatrix} x \\ y \\ z \end{pmatrix} \right] \cdot \frac{\partial \mathbf{r}^i_{\text{tLA}}}{\partial p_j} . \tag{9}$$

In order to compute the sub-pixel DTM heights $r^i_{\text{DTM}}(\lambda, \phi)$ and the height gradients $\partial r^i_{\text{DTM}}/\partial\lambda$ and $\partial r^i_{\text{DTM}}/\partial\phi$, an interpolation technique is applied. The nearest DTM grid element to the coordinates of the laser footprint (λ, ϕ) is treated as the central grid element. The eight neighboring pixels surrounding the central pixel are used for interpolation. Height differences on the edge of the DTM or in the vicinity of data gaps that do not have eight neighbors are discarded. As described in Section 4.2, the effective resolution of the DTM is approximately an order of magnitude larger than the size of the DTM grid elements. Thus, the topography within the 3×3 patch is sufficiently described by a sloped plane, the

parameters of which are determined by a least-squares estimation. From the fitted plane, sub-pixel DTM heights can be extracted at any coordinate pair, and the normal vector of the plane gives the required gradient.

The height differences $\mathbf{g}(\mathbf{p}) = (g^1(\mathbf{p}), \ldots, g^n(\mathbf{p}))$ may contain extreme outliers, caused, for example, by false detections of laser pulses, or small-scale topographic features (e.g., craters) not seen in the stereo DTM. These points can substantially bias the co-registration procedure. Thus, we exclude all observations that are predicted to occur with a probability of less than 1% (3σ threshold). For the initial iteration, the threshold is set to 5 km. At each subsequent iteration step, the threshold criterion is reevaluated to see if measurements that were excluded at the beginning could be incorporated into subsequent co-registration steps.

Because the co-registration is a non-linear method, and thus requires an initial guess of the solution parameters, we initialized the parameters with the assumed (current best estimates) values and performed five iterations to let the parameters evolve to their final values. Given that the improvement in the root mean square (RMS) residual for the subsequent iteration was under the centimeter level, we found five iterations to be sufficient. Starting from different initial values did not change the results but increased the number of iterations needed.

6 Data weighting and error estimation

The data used in the co-registration can be weighted in a variety of ways to account for the quality of the measurements. Laser altimeter measurements performed on sloped surfaces, for instance, or at off-nadir orientations are prone to higher errors in the range estimation. These uncertainties can be considered through the covariance of the height differences $\mathbf{C}_g$. Our observations are the inertial laser altimeter footprint coordinates and DTM heights, and we must propagate the uncertainties in the observations to the height differences. The observations vector $\mathbf{h}$ is composed of

$$\mathbf{h} = \left(\lambda^1_{\text{iLA}}, \ldots, \lambda^n_{\text{iLA}}, \phi^1_{\text{iLA}}, \ldots, \phi^n_{\text{iLA}}, r^1_{\text{iLA}}, \ldots, r^n_{\text{iLA}}, r^1_{\text{DTM}}, \ldots, r^m_{\text{DTM}}\right) , \tag{10}$$

where $(\lambda_{\text{iLA}}, \phi_{\text{iLA}}, r_{\text{iLA}})$ are the coordinates and height of the laser footprint in the inertial frame and r^i_{DTM} are the DTM heights used in the interpolation of the sub-pixel DTM heights. Individual DTM heights can be used to compute more than one observation as a result of the interpolation technique applied to the DTM. Thus, the number of DTM pixels m is different from the number of laser footprints n. This situation leads to a block structure of the weighting matrix and reflects correlations among the observations. To calculate the weighting matrix $\mathbf{C}_g$ we

have to propagate the errors in the observed quantities to the height differences by means of

$$\mathbf{C}_g = \mathbf{T}_h^{\mathrm{T}} \mathbf{C}_h \mathbf{T}_h \,, \tag{11}$$

where $\mathbf{T}_h$ is the matrix of partial derivatives $[\mathbf{T}_h]_{ij} = \partial g^i / \partial h_j$ of the height differences with respect to the observations $\mathbf{h}$, and $\mathbf{C}_h$ is the covariance of the observations. The variances of the observations are

$$\sigma^2(\lambda^i_{\mathrm{iLA}}) = \frac{(r^i_{\mathrm{s/c}}\sigma_p)^2 + (\sigma_{o\lambda})^2}{R^2} \,, \tag{12}$$

$$\sigma^2(\phi^i_{\mathrm{iLA}}) = \frac{(r^i_{\mathrm{s/c}}\sigma_p)^2 + (\sigma^2_{o\phi})^2}{(R\cos\lambda^i)^2} \,, \tag{13}$$

$$\sigma^2(r^i_{\mathrm{iLA}}) = (\sigma_{or})^2 + (\sigma^i_h)^2 \,, \tag{14}$$

where $r^i_{\mathrm{s/c}}$ is the range distance from the spacecraft (s/c) to the laser footprint, and $R = 2440\,\mathrm{km}$ is Mercury's mean radius. We set the uncertainties in the observations according to the simulation (see Section 4). The pointing error is $\sigma_p = 560\,\mu\mathrm{rad}$, the lateral orbit error is $\sigma_{o\lambda} = \sigma_{o\phi} = 250\,\mathrm{m}$, and the radial orbital error is $\sigma_{or} = 10\,\mathrm{m}$. $\sigma^i_h = r^i_{\mathrm{s/c}}\sigma_p \sin\varphi^i$ for an off-nadir angle φ^i. The DTM pixel error is $\sigma(r^i_{\mathrm{DTM}}) = 60\,\mathrm{m}$.

The quantity $\mathbf{C}_p = (\mathbf{G}^{\mathrm{T}}\mathbf{C}_g^{-1}\mathbf{G})^{-1}$ gives the precision achievable with the given data but provides no information on the accuracy of the solved parameters. However, we can estimate the accuracy of the proposed method and the underlying data by performing several simulations and calculating the differences between the estimated and the assumed rotational parameters.

We performed 100 different simulations of laser altimeter measurements and estimated the covariance from

$$\left[\hat{\mathbf{C}}_p\right]_{ij} = \frac{1}{99}\sum_{n=1}^{100}(p^n_i - p^*_i)(p^n_j - p^*_j) \,, \tag{15}$$

where p^n_i is the value of the ith parameter of the nth simulation, and p^*_j is the jth assumed parameter. The expected value $\hat{\mathbf{p}}$ of the parameters from the simulations is obtained from $\hat{\mathbf{p}} = 1/100\sum_{n=1}^{100}\mathbf{p}^n$. Comparison of the error estimates derived from $\hat{\mathbf{C}}_p$ with the errors derived from the formal covariance $\mathbf{C}_p$ shows that the formal errors underestimate the actual errors by a factor of 20.

7 Results

A comparison of the "assumed" parameters p^* with the parameters "estimated" from the simulations $\hat{\mathbf{p}}$ as well as the parameter errors obtained with Eq. 15 are shown in Table 1. The results indicate that the rotational parameters were determined with high accuracy. The orientation of the spin axis was estimated with an

Table 1: Simulated and estimated values for the rotational parameters.

	simulated	estimated	error (1σ)
α_0 [°]	281.001030	281.0101	0.0012
δ_0 [°]	61.41550	61.41578	0.00072
ω_1 [°/day]	6.1385025	6.1385025	0.0000038
g_{88} [arc sec]	38.5	38.1	4.6

Notes: α_0 and δ_0 define the orientation of the spin axis at J2000.0, ω_1 is the spin rate, and g_{88} is the libration amplitude. The assumed values are taken from the most recent observations by Earth-based radar (*Margot et al.*, 2012). The estimated 1σ errors were calculated from Eq. 15. The precession rates α_1 and δ_1 as well as the prime meridian ω_0 were treated as constants.

accuracy of approximately 3 arc sec. Converting the coordinates of the rotation axis to the obliquity, we obtain (2.024 ± 0.042) arc min, a value in agreement with the simulated value of 2.041 arc min.

The spin rate parameter ω_1 contains the highest number of significant figures among the parameters and again shows very good agreement between simulated and assumed values. The estimated 1σ uncertainty is only 5 arc sec per year. Thus with the stable body-fixed reference provided through the stereo DTM, it is possible to measure precisely the spin rate and even track its small variation with time, i.e., the libration in longitude. The libration amplitude g_{88} has an estimated uncertainty of 4.6 arc sec, which corresponds to only 54 m at the equator. Hence, we can confirm that our method and the given data set lead to accurate estimations.

The co-registration involves 11 parameters (four rotational and seven similarity transformation parameters) determined from about 2.16 million of observed height differences. To study the performance of the co-registration we show the height differences before and after co-registration (Fig. 4). The RMS height difference was initially 205 m and decreased to 96 m after co-registration. This final height difference RMS is consistent with the RMS value for simulated heights of 92 m. Furthermore, it can be observed in Fig. 4 that tilts and vertical offsets are minimized during the co-registration process. The lateral offsets between the data sets, which cause relief-like signatures in the height residuals, are removed as well. It is worthwhile to determine the number of observations required to obtain a given accuracy for the parameter estimates. The significance of a parameter in a regression is determined by its $t-\text{statistic} = \Delta p_i / \sqrt{[\hat{\mathbf{C}}_p]_{ii}}$, where Δp_i is a defined significance of the ith parameter and $[\hat{\mathbf{C}}_p]_{ii}$ the corresponding estimated variance. We define the significance levels (95%) as follows: 30 arc sec for the right ascension α_0, 15 arc sec for the declination δ_0, 15 arc sec for the libration

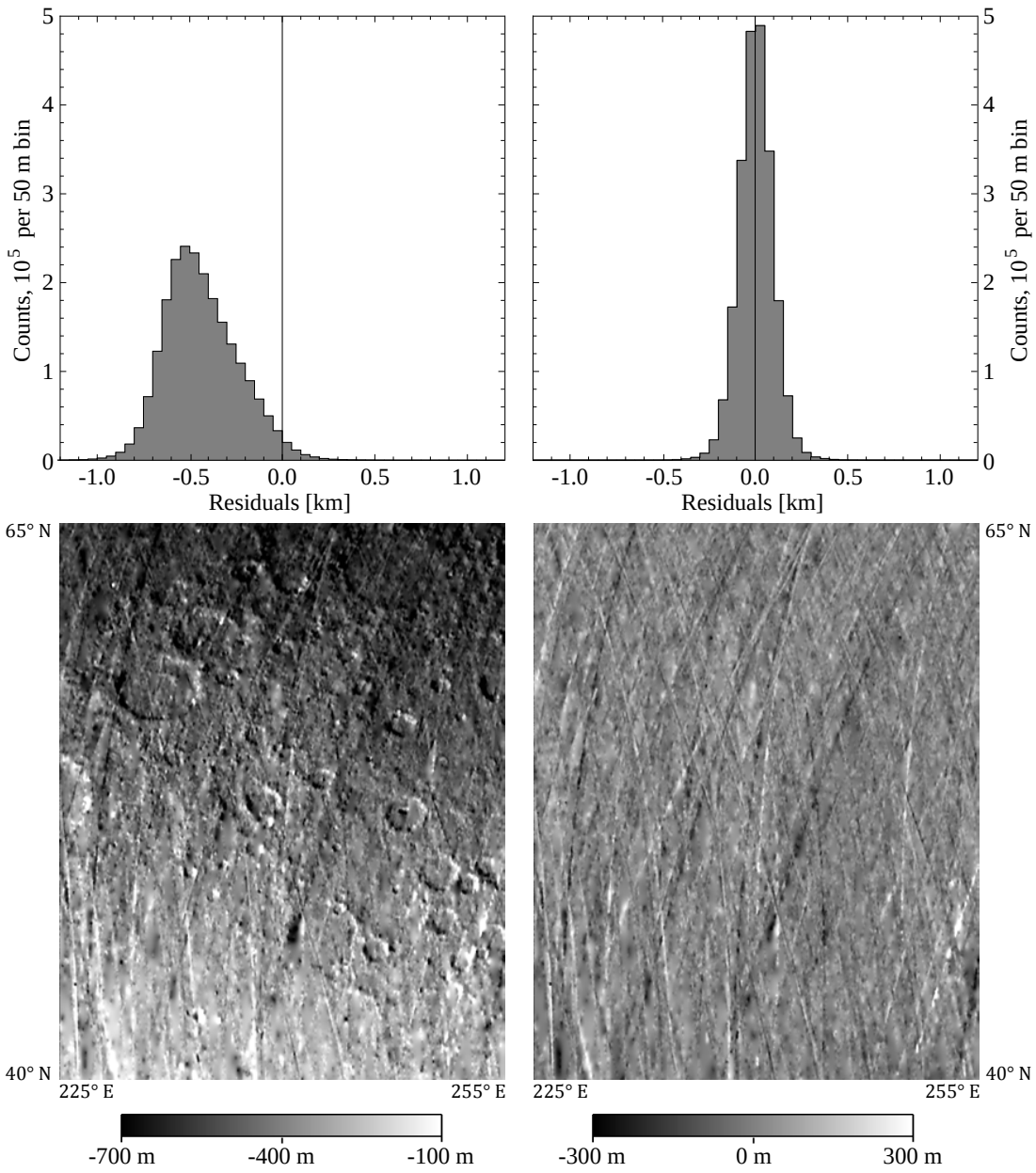

Figure 4: Histogram and map of height residuals before (left) and after (right) co-registration. The map shows the same region as in Fig. 2.

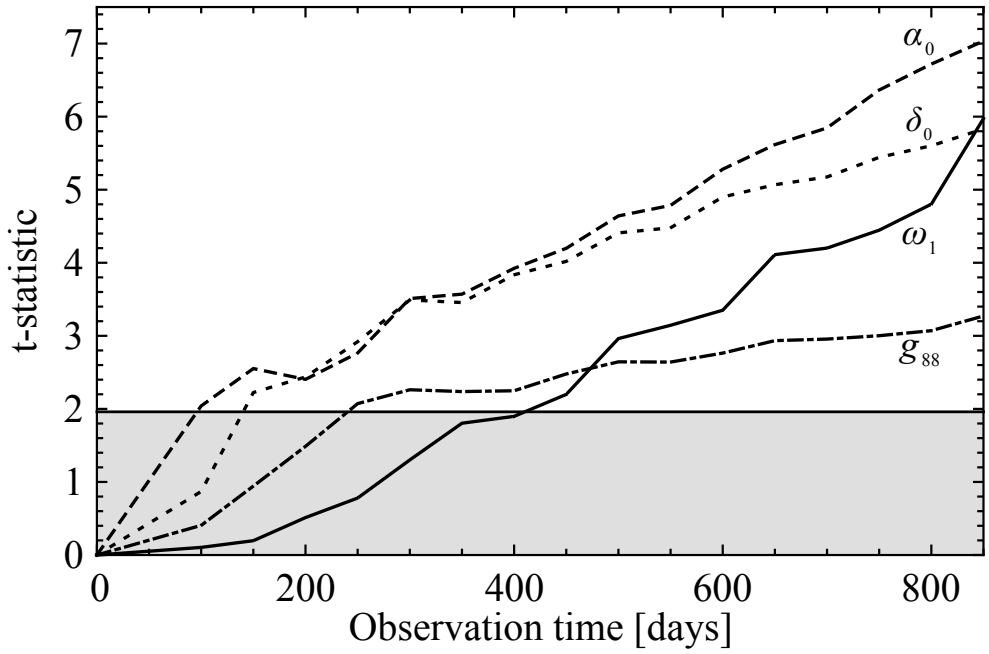

Figure 5: t-statistic of rotational parameters as a function of observation time (dashed: α_0; dotted: δ_0 solid: ω_1; dot-dashed: g_{88}). The parameter significance values are defined in the text. The gray shaded area indicates significance levels less than 95%.

amplitude g_{88}, and 30 arc sec per year (0.000023° / day) for the spin rate ω_1. Fig. 5 visualizes the t-statistic as a function of observation time for the several rotational parameters. The error estimates were obtained with Eq. 15 and appropriately shortened versions of the 100 simulations of laser altimeter measurements. The step size was thereby 50 days (almost one Mercury rotation period). A correction of 15 arc sec (177 m) in the pole position reaches a 95% level of significance after an observing time of approximately 150 (Earth) days. The spin rate and the libration amplitude require the longest observing times (approximately 400 and 250 days, respectively) to become significant at the defined levels. Thus, observation times of several Mercury sidereal days are mandatory to determine precisely the rotation rate and its small oscillations. Whereas the significance of the libration amplitude parameter increases only slowly over time, the spin rate estimation improves quickly, benefiting from any included observations. Note that the significance of the rotational parameters is not only a function of the observing time but also of DTM quality. A stereo DTM with a higher resolution or higher spatial coverage would lead to more accurate estimates within a given observation time.

8 Discussion and conclusion

We have demonstrated that it is feasible to determine Mercury's rotational parameters from image and laser altimeter data acquired by the MESSENGER spacecraft. An extensive simulation of observational data verified that the parameters are estimated correctly by our method.

As an additional benefit, our approach allows the establishment of a global control for individual stereo topographic models by connection through laser altimeter profiles or sparse topographic data, e.g., limb profiles (*Elgner et al.*, 2014) in the southern hemisphere, where MLA data are not generally available. Although the co-registration method transforms the control points (laser or limb profiles) into the reference frame of the DTM, it is straightforward to compute the inverse transformation that transforms the DTM to the control points. Once co-registration is performed, it is easy to detect outliers and achieve improvements in either of the two data sets. Additional observations, e.g., height differences at intersecting laser profiles (cross-overs), in combination with the co-registration to the stereo DTM, can lead to a substantial increase in the accuracy of the rotational parameters.

The actual data collected by the MESSENGER spacecraft corresponds to a single run of the simulation performed in this study. Thus, the measurements once obtained by the spacecraft cannot be repeated, and any systematic errors may not be evident. We do not correct for systematic errors, but rather we assume that over a long time span the effect of the systematic errors on the rotational parameters can be approximated as random. With the method of this paper we could learn how these errors translate into uncertainties in the rotational parameters and verify that the estimated parameters are unbiased. Usage of additional stereo DTMs (*Preusker et al.*, 2014) at different locations on Mercury can substantially increase the precision of the estimation. The determination of the orientation of the spin axis can benefit in particular from the extensive MLA coverage at high northern latitudes. Furthermore, a detailed study of the quality of the observational data can be expected to improve the results of parameter estimation. Visual inspection of the height residuals may help to identify systematic errors or outliers.

We see great potential for the method presented here for determining rotational parameters of Mercury from MESSENGER data. Moreover, the formalism developed here is also suitable for other celestial bodies, for which laser altimetry data in combination with stereo topographic models are available or will be in the near future.

Acknowledgments

This research was funded by a grant from the German Research Foundation (OB124/11-1). The MESSENGER mission is supported by the NASA Discovery Program under contract NAS5-97271 to The Johns Hopkins University Applied Physics Laboratory and NASW-00002 to the Carnegie Institution of Washington. We thank two anonymous reviewers for their thoughtful comments on an earlier version of the manuscript. The authors thank Philipp Gläser, Hauke Hussmann, and Erwan Mazarico for helpful comments and discussions. J. Oberst greatly acknowledges being hosted by MIIGAiK and supported by the Russian Science Foundation under Project 14-22-00197.

Reprinted from *Mercury's rotational parameters from MESSENGER image and laser altimeter data: A feasibility study*, Stark, A., Oberst, J., Preusker, F., Gwinner, K., Peale, S.J., Margot, J.-L., Phillips, R.J., Zuber, M.T., Solomon, S.C., Planetary and Space Science, 117, 64-72, Copyright (2015), with permission from Elsevier.

References

Archinal, B. A., et al. (2011), Report of the IAU Working Group on Cartographic Coordinates and Rotational Elements: 2009, *Celestial Mechanics and Dynamical Astronomy*, *109*(2), 101–135.

Baltsavias, E. P. (1999), A comparison between photogrammetry and laser scanning, *ISPRS Journal of Photogrammetry and Remote Sensing*, *54*(2-3), 83–94.

Cavanaugh, J. F., et al. (2007), The Mercury Laser Altimeter instrument for the MESSENGER mission, *Space Science Reviews*, *131*(1-4), 451–479.

Cicalò, S., and A. Milani (2012), Determination of the rotation of Mercury from satellite gravimetry, *Monthly Notices of the Royal Astronomical Society*, *427*(1), 468–482.

Elgner, S., A. Stark, J. Oberst, M. E. Perry, M. T. Zuber, M. S. Robinson, and S. C. Solomon (2014), Mercury's global shape and topography from MESSENGER limb images, *Planetary and Space Science*, *103*, 299–308.

Gläser, P., I. Haase, J. Oberst, and G. A. Neumann (2013), Co-registration of laser altimeter tracks with digital terrain models and applications in planetary science, *Planetary and Space Science*, *89*(0), 111–117.

Gwinner, K., et al. (2010), Topography of Mars from global mapping by HRSC high-resolution digital terrain models and orthoimages: Characteristics and performance, *Earth and Planetary Science Letters*, *294*(3-4), 506–519.

Habib, A., and T. Schenk (1999), A new approach for matching surfaces from laser scanners and optical scanners, in *Mapping Surface Structure and Topography by Airborne and Spaceborne Lasers*, vol. 32-3/W14, edited by B. M. Csatho, International Archives of the Photogrammetry, Remote Sensing and Spatial Information Societies, 7 pp.

Hauck, S. A., II, et al. (2013), The curious case of Mercury's internal structure, *Journal of Geophysical Research: Planets*, *118*(6), 1204–1220.

Hawkins, S. E., III, et al. (2007), The Mercury Dual Imaging System on the MESSENGER spacecraft, *Space Science Reviews*, *131*(1-4), 247–338.

Jehn, R., C. Corral, and G. Giampieri (2004), Estimating Mercury's 88-day libration amplitude from orbit, *Planetary and Space Science*, *52*(8), 727–732.

Kaula, W. M. (2000), *Theory of Satellite Geodesy: Applications of Satellites to Geodesy*, 36-38 pp., Dover, Mineola, N.Y., 160 p.

Koch, C., U. Christensen, and R. Kallenbach (2008), Simultaneous determination of global topography, tidal Love number and libration amplitude of Mercury by laser altimetry, *Planetary and Space Science*, *56*(9), 1226–1237.

Koch, C., R. Kallenbach, and U. Christensen (2010), Mercury's global topography and tidal signal from laser altimetry by using a rectangular grid, *Planetary and Space Science*, *58*(14-15), 2022–2030.

Lin, S. Y., J. P. Muller, J. P. Mills, and P. E. Miller (2010), An assessment of surface matching for the automated co-registration of MOLA, HRSC and HiRISE DTMs, *Earth and Planetary Science Letters*, *294*(3-4), 520–533.

Margot, J. L. (2009), A Mercury orientation model including non-zero obliquity and librations, *Celestial Mechanics and Dynamical Astronomy*, *105*(4), 329–336.

Margot, J. L., S. J. Peale, R. F. Jurgens, M. A. Slade, and I. V. Holin (2007), Large longitude libration of Mercury reveals a molten core, *Science*, *316*(5825), 710–714.

Margot, J. L., et al. (2012), Mercury's moment of inertia from spin and gravity data, *Journal of Geophysical Research-Planets*, *117*(E12), E00L09.

Mazarico, E., A. Genova, S. Goossens, F. G. Lemoine, G. A. Neumann, M. T. Zuber, D. E. Smith, and S. C. Solomon (2014), The gravity field, orientation, and ephemeris of Mercury from MESSENGER observations after three years in orbit, *Journal of Geophysical Research-Planets*, *119*(12), 2417–2436.

Peale, S. J. (1976), Does Mercury have a molten core, *Nature*, *262*(5571), 765–766.

Peale, S. J. (1988), The rotational dynamics of mercury and the state of its core, in *Mercury*, edited by F. Vilas, C. R. Chapman, and M. S. Matthews, pp. 461–493, University of Arizona Press, Tucson, Ariz.

Peale, S. J., M. Yseboodt, and J. L. Margot (2007), Long-period forcing of Mercury's libration in longitude, *Icarus*, *187*(2), 365–373.

Pfyffer, G., T. Van Hoolst, and V. Dehant (2011), Librations and obliquity of Mercury from the BepiColombo radio-science and camera experiments, *Planetary and Space Science*, *59*(9), 848–861.

Postolov, Y., A. Krupnik, and K. McIntosh (1999), Registration of airborne laser data to surfaces generated by photogrammetric means, in *Mapping Surface Structure and Topography by Airborne and Spaceborne Lasers*, vol. 32-3/W14, edited by B. M. Csatho, p. 5 pp., International Archives of the Photogrammetry, Remote Sensing and Spatial Information Societies.

Preusker, F., J. Oberst, J. W. Head, T. R. Watters, M. S. Robinson, M. T. Zuber, and S. C. Solomon (2011), Stereo topographic models of Mercury after three MESSENGER flybys, *Planetary and Space Science*, *59*(15), 1910–1917.

Preusker, F., A. Stark, J. Oberst, K. J. Becker, M. E. Perry, and S. C. Solomon (2014), Topography of Mercury: A global model from MESSENGER orbital stereo mapping, *European Planetary Science Congress 2014*, *EPSC2014-709*.

Rosat, S., P. Rosenblatt, A. Trinh, and V. Dehant (2008), Mars and Mercury rotation variations from altimetry crossover data: Feasibility study, *Journal of Geophysical Research-Planets*, *113*(E12), E12,014.

Santo, A. G., et al. (2001), The MESSENGER mission to Mercury: spacecraft and mission design, *Planetary and Space Science*, *49*(14-15), 1481–1500.

Smith, D. E., M. T. Zuber, X. Sun, G. A. Neumann, J. F. Cavanaugh, J. F. McGarry, and T. W. Zagwodzki (2006), Two-way laser link over interplanetary distance, *Science*, *311*(5757), 53.

Smith, D. E., et al. (2012), Gravity field and internal structure of Mercury from MESSENGER, *Science*, *336*(6078), 214–217.

Srinivasan, D. K., M. E. Perry, K. B. Fielhauer, D. E. Smith, and M. T. Zuber (2007), The radio frequency subsystem and radio science on the MESSENGER mission, *Space Science Reviews*, *131*(1-4), 557–571.

Stark, A., J. Oberst, and H. Hussmann (2015), Mercury's resonant rotation from secular orbital elements, *Celestial Mechanics and Dynamical Astronomy*, *123*(3), 263–277.

Tarantola, A., and B. Valette (1982), Generalized nonlinear inverse problems solved using the least squares criterion, *Reviews of Geophysics*, *20*(2), 219.

Wu, B., J. Guo, H. Hu, Z. L. Li, and Y. Q. Chen (2013), Co-registration of lunar topographic models derived from Chang'E-1, SELENE, and LRO laser altimeter data based on a novel surface matching method, *Earth and Planetary Science Letters*, *364*(0), 68–84.

Wu, X., P. L. Bender, S. J. Peale, G. W. Rosborough, and M. A. Vincent (1997), Determination of Mercury's 88 day libration and fluid core size from orbit, *Planetary and Space Science*, *45*(1), 15–19.

Yseboodt, M., and J. L. Margot (2006), Evolution of Mercury's obliquity, *Icarus*, *181*(2), 327–337.

Yseboodt, M., J. L. Margot, and S. J. Peale (2010), Analytical model of the long-period forced longitude librations of Mercury, *Icarus*, *207*(2), 536–544.

Zuber, M. T., et al. (2008), Laser Altimeter observations from MESSENGER's first Mercury flyby, *Science*, *321*(5885), 77–79.

Zuber, M. T., et al. (2012), Topography of the Northern Hemisphere of Mercury from MESSENGER Laser Altimetry, *Science*, *336*(6078), 217–220.